Heteroatom Chemistry

WILEY

RESEARCH ARTICLE OPEN ACCESS

Synthesis and Characterization of Novel (Substituted-Phenyl)-(5-Methoxy-2-Phenyl-1H-1, 3-Benzimidazol-1-yl) Methanone Derivatives and Evaluation of Anticancer Activity

Ranjeeta Verma[1] | Shweta Verma[1] | Nahid Abbas[2]

[1]Department of Pharmaceutical Chemistry, IFTM University, Moradabad, India | [2]Department of Pharmaceutical Chemistry, Akshaya Institute of Pharmacy, Tumkur Affiliated to Rajiv Gandhi University of Health Science, Bengaluru, India

Correspondence: Nahid Abbas (drnahidabbas@gmail.com)

Received: 4 August 2025 | **Revised:** 4 February 2026 | **Accepted:** 12 February 2026

Academic Editor: Arnab Biswas

Keywords: 5-methoxy aryl derivatives | anticancer activity | A549 | benzimidazole | HeLa | IC_{50} | MCF-7

ABSTRACT

A series of 5-methoxy aryl benzimidazole derivatives were designed and synthesized using a simple two-step facile method. The novel benzimidazole derivatives were characterized through FT-IR, ^{1}H-NMR,^{13}C-NMR, and LC-MS. The synthesized compounds (**C1–C9**) were screened for their *in vitro* anticancer activity against MCF-7 (human breast adenocarcinoma), HeLa (cervical cancer), and A549 (non–small-cell lung carcinoma) cell lines using cell viability assays. These cell lines exhibit high basal surface expression of EGFR, the cytotoxic effects were evaluated over a broad concentration range (0.625 to 300 μg/mL), and the IC_{50} values were determined. Doxorubicin was used as a standard reference drug for comparison. In the designed 5-methoxy aryl benzimidazole derivatives, C1 and C7 were the top hits in molecular docking. They had better interaction than the standard reference, with interaction energies of −9.280 and −9.250 kcal/mol, respectively. They had hydrogen bond interactions with THR798 and MET801 at the ATP-binding site of EGFR kinase.

Among the tested compounds, C7 and C1 demonstrated significant anticancer activity, showing potent growth inhibition with an IC50 value of 9.2 ± 0.5 μM against the MCF-7 cell line, highlighting its potential as a strong candidate for breast cancer therapy. Similarly, Compound C1 demonstrated notable potency against the A549 cell line, with an IC50 value of 16.6 ± 2.3 μM. These novel 5-methoxy aryl benzimidazole derivatives exhibited potent anticancer activity.

1 | Introduction

Cancer is a disease that led to 9.6 million deaths in the previous decade [1]. It has been reported that females commonly suffer from breast, stomach, liver, bone, lung, colon, leukemia, and cervical cancer [2]. The World Health Organization (WHO) statistics state that cancer has increased mortality worldwide. Among 19.3 million reported cancer cases in 2020, 2.3 million were for breast cancer. Breast cancer is the most common malignancy in women and is a heterogeneous disease at the molecular level. Over the past 10–15 years, treatment concepts have evolved to take this heterogeneity into account. Emphasis was laid on biologically directed therapies and treatment by de-escalation to reduce the adverse effects of treatment [3].

The early stage of breast cancer, in which the cancer is in the breast or has spread to the auxiliary lymph nodes, is curable. Improvements in multimodal therapy have led to an increasing

opportunity to cure in 70%–80% of patients. In contrast, advanced breast cancer is also a treatable disease. Breast cancer treatment has significantly improved over the years with the introduction of targeted therapies, chemotherapy, radiation therapy, and surgical interventions. The choice of treatment depends on the stage, molecular subtype, and patient characteristics. Hormone receptor–positive breast cancers are treated with endocrine therapy, while HER2-positive cancers benefit from HER2-targeted therapies, such as trastuzumab. Triple-negative breast cancer (TNBC), which lacks estrogen, progesterone, and HER2 receptors, remains a challenge due to limited targeted therapy options. Despite these advancements, drug resistance, adverse effects, and recurrence remain significant issues in breast cancer management. Therefore, researchers continue to explore novel therapeutic strategies, including small molecules, nanoparticles, and natural compounds, to enhance efficacy and minimize toxicity [4].

Benzimidazole derivatives exhibit structural similarity to purine, allowing them to interact with biological targets effectively. Their ability to inhibit enzymes, disrupt DNA replication, and induce apoptosis in cancer cells makes them promising candidates for anticancer drug development. Recent studies have demonstrated that benzimidazole derivatives can target various oncogenic pathways, including inhibition of tubulin polymerization, DNA intercalation, and modulation of kinase activity. These derivatives are important medicines for PPI inhibition, antifungal, antihistamine, antihypertensive, and anthelmintics [5].

Small molecules with benzimidazole nucleus produce minimal toxicity; hence, it is an excellent scaffold for the development of anticancer agents. Benzimidazole (also known as 1*H* –benzimidaole,1,3-benzodiazole, benzogloxaline, iminazole, and imidazole) is made up of an aromatic benzene ring fused with an imidazole ring at the 4,5 position. The proton on the first nitrogen exhibits tautomerism after aprotic solvent interaction [6].

The drugs, such as mebendazole and flubendazole, have a benzimidazole scaffold though anthelmintics and antiparasitics were repurposed. These anthelmintics displayed profound anticancer activity by inhibiting tubulin in breast cancer.

Epidermal growth factor receptor (EGFR) has been investigated for breast, lung, gastric, prostate, and other cancers. Currently, lapatinib is an approved drug for breast cancer. Therefore, this research was an attempt to design small molecules with benzimidazole core for EGFR kinase inhibition to treat breast cancer.

Among the US Food and Drug Administration (FDA)-approved drug, benzimidazole heterocycles are among the top ten [7]. The designed benzimidazole derivatives were capable of fitting into the receptors' ATP-binding site. Table 1 displays clinically approved drugs with benzimidazole scaffold.

The designed aryl-5-methoxy benzimidazole derivatives were synthesized by using the two-step facile method as described in the scheme. The small molecules were characterized through FT-IR, ^{1}H-NMR, ^{13}C-NMR, and HRMS. The synthesized compounds (C1–C9) were screened for their *in vitro* anticancer activity against MCF-7 (human breast adenocarcinoma), HeLa (cervical cancer), and A549 (non–small cell lung carcinoma) cell lines using cell viability assays. Doxorubicin was used as a standard reference drug for comparison.

2 | Materials and Methods

2.1 | Molecular Docking

2.1.1 | Protein Preparation

The 3D structure of the protein EGFR kinase with the PDB ID 3 W2S and 3RCD was obtained from the Protein Data Bank via the Protein Preparation. The 3RCD and 3 W2S are EGFR proteins having pyrrolo [3,2-d]pyrimidine scaffold ligand which was replaced by newly designed benzimidazole derivatives (Wizard in Maestro). Several preprocessing steps were applied to the protein, including assigning bond orders, removing original hydrogens, adding hydrogens, establishing zero-order bonds to metals, forming disulfide bonds, converting seleno-methionines to methionines, addressing missing side chains and loops through Prime, eliminating water molecules farther than 5 Å from hetero groups, and generating het states using Epik at pH 7.0 ± 2.0. Subsequently, the protein underwent refinement, involving H-bond assignment through sampling water orientations, employing PROPKA at pH 7.0, and optimizing its structure. The protein was further subjected to restrained minimization utilizing the OPLS3 force field as described in previous works.

2.1.2 | Receptor Grid Generation

Following protein preparation, a receptor grid with dimensions of 20 Å was created. This grid was centered on the active site, using the cocrystallized ligand as the reference point.

2.1.3 | Preparation of Ligand

All molecules were constructed, converted into 3D structures, and subjected to energy minimization using the Ligprep and Confgen functions within Maestro. The resulting library was then saved in the maegz format.

2.1.4 | Molecular Docking

Next, molecular docking was conducted using the Glide program with the Standard Precision (SP) algorithm to assess the interactions between proteins and ligands and determine their binding affinities. For this investigation, the options to include Epik state penalties in the docking score and enhance the planarity of conjugated pi group functions were chosen. To validate the molecular docking, a re-docking procedure was performed with the cocrystallized ligand placed within the grid, and the resulting root-mean-square deviation (RMSD) of 0.197 was deemed acceptable for validation purposes.

2.1.5 | Synthesis of Aryl-5-Methoxy Benzimidazole

The synthesis of aryl-5-methoxy benzimidazole was carried out using a simple and effective chemical method. In this procedure, 4-methoxy benzene-1,2-diamine (1 mmol) was added to ammonium chloride (4 mmol) in the presence of chloroform (5 mL) and stirred for 5 min. Subsequently, benzaldehyde (1 mmol) was introduced into the reaction mixture and stirred continuously for 4 h. The reaction progress was monitored using thin-layer chromatography (TLC) with a mobile phase consisting of n-hexane and ethyl acetate (1:5). On completion of the reaction, the solvent was removed, and the residue was transferred to a separating funnel. Dichloromethane (20 mL) was added to the reaction mixture, followed by washing the organic layer with

TABLE 1 | Structures, biological targets, and applications of clinically approved drugs with benzimidazole scaffold as found in https://www.drugs.com.

Compound code	Structure	Current status	Target	Application
Mebendazole	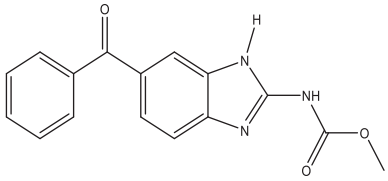	Sold as Vermox	Repurposed drug inhibits tubulin polymerization	To treat breast cancer, repurposed anthelmintic drug
Flubendazole	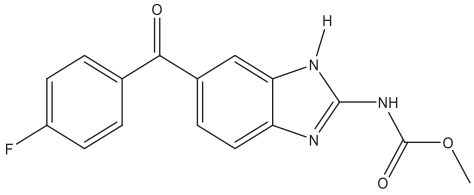	Sold as Zelcom	Repurposed drug inhibits tubulin polymerization	To treat breast cancer, repurposed anthelmintic drug
Bendamustine (NCT04217317 and NCT04510636)	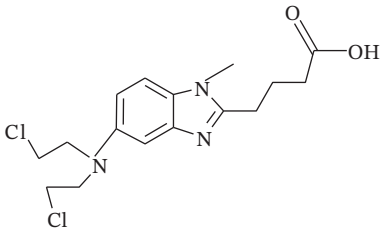	Sold as Treanda	It is an *alkylating agent* $IC_{50} = 50\ \mu M$	Chronic lymphocytic leukemia
Selumetinib (NCT02768766)	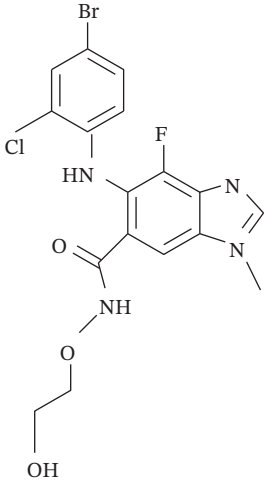	Sold as Koselugo	It is selective, non-ATP-competitive oral MEK1/2 inhibitor $IC_{50} = 14\ nM$	To treat neurofibromatosis type 1
Abemaciclib (NCT04003896 and NCT0404-0205)	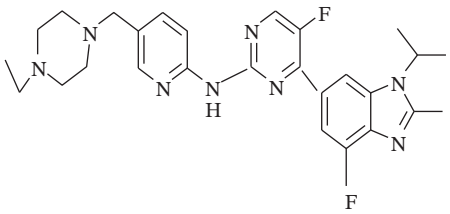	Sold as Verzenio	It is more selective toward CDK4 $IC_{50} = 2\ nM$ than CDK6 $IC_{50} = 25\ nM$	HR-positive and HER2-negative breast cancer
Pracinostat (NCT03848754)	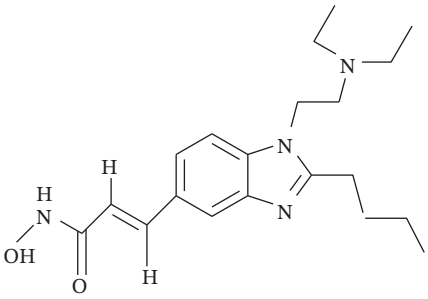	Phase III trial	Pracinostat (SB939) is a potent pan-HDAC (histone deacetylase) inhibitor with $IC_{50} = 40\ nM$	Treatment of advanced solid tumors and AML

(Continues)

TABLE 1 | (Continued)

Compound code	Structure	Current status	Target	Application
Dovitinib (NCT01635907)	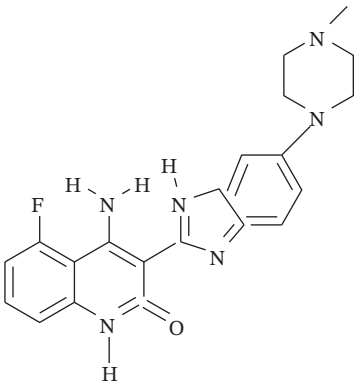	Phase II trial	Potent multitargeted tyrosine kinase (RTK) inhibitor with $IC_{50} = 27$ nM	Treat AML

10 mL of water. After separating the aqueous and organic layers into separate beakers, the organic layer was dried to obtain the desired product. The final compounds, substituted aryl-5-methoxy benzimidazole, were purified by silica gel (60–120 mesh) column chromatography using EtOAc–n-hexane (4:6 to 8:2 v/v) as the eluent, affording the analytically pure product, and were characterized. This method provided a high yield of the synthesized compounds with significant purity and stability. The refined synthesis approach ensured efficient formation of benzimidazole derivatives with potential pharmacological applications [8, 9].

2.1.6 | Procedure for the Synthesis of 1H-[d] Imidazole-1-yl) (Aryl) Methanones

An oven-dried round-bottom flask was charged with a solution of K_2CO_3 (2 mmol) in DMF (10 mL). To this solution, 5-methoxy-2-phenyl-1H-benzo[d]imidazole (1) (1.0 mmol) and substituted benzoyl chlorides (2) (1.1 mmol) were added. The reaction mixture was stirred and heated at 80°C in an oil bath for 4–6 h. After completion, the mixture was cooled to room temperature and concentrated under vacuum. The crude product was purified by silica gel (60–120 mesh) column chromatography using EtOAc–n-hexane (4:6 to 8:4 v/v) as the eluent, affording the analytically pure product [10] Scheme 1 Table 2.

2.1.7 | Synthesis and Characterization

The designed compounds with top in silico scores were taken up for synthesis. The feasibility of chemicals, reaction conditions, and synthetic schemes was considered and planned accordingly.

2.1.7.1 | Reagents and Instruments. Unless otherwise noted, all reagents and solvents were of commercial quality and utilized without further purification. TLC was used to monitor the reaction's progress, and the spots were seen under UV illuminations of 254 nm (short wavelength) and 365 nm (long wavelength) using Merck 60 F 254 silica gel plates. The FT-IR spectra were recorded using the KBr pellet procedure by the IR-Prestige 21, Shimadzu Corpn., Japan. Melting points were recorded on digital OptiMelt (Stanford Research System). The ^{1}H NMR and ^{13}C NMR spectra were recorded using JEOL Delta Nuclear Magnetic Resonance spectrometer at 400 and 100 MHz, respectively, with TMS as an internal standard. The ^{1}H NMR and ^{13}C NMR spectra were recorded in solvent CDCl3, with 1H and 13C NMR peaks at 7.26 and 77.00 ppm, respectively, in solvent DMSO-d6 at 2.50 and 39.51 ppm, respectively, and in solvent MeOD at 4.87 and 49.1 ppm, respectively. Coupling constants were reported in hertz (Hz). The abbreviations used to characterize the signals are as follows: s = singlet, m = multiplet, d = doublet, dd = doublet of doublet, dt = doublet of triplet, t = triplet, q = quartet. Mass spectra were recorded using ESI mode by the Ultimate 3000, Thermo Scientific, USA. Column chromatography was performed using Merck silica gel (60–120 mesh).

2.1.8 | In Vitro Anticancer Activity Evaluation Against MCF-7, HeLa, and A549 Cell Lines

The synthesized test compounds **(C1–C9)** were systematically evaluated for their in vitro anticancer activity against three human cancer cell lines: MCF-7 (human breast adenocarcinoma), HeLa (cervical cancer), and A549 (non–small cell lung carcinoma, NSCLC). Cell line common names (cell line official name, RRID number) are as follows: MCF-7 (ATCC HTB-22, RRID:CVCL_0031), HeLa (ATCC CCL-2, RRID:CVCL_0030), and A549 (ATCC CCL-185, RRID:CVCL_0023). These cell lines were selected based on their clinical relevance and widespread use as models in anticancer research. These cell lines express EGFR. They express physiological levels of EGFR estimates ranging from 40,000 to 100,000 receptors per cell. These cell lines were procured from the National Centre for Cell Science (NCCS), Pune, an autonomous organization aided by the Department of Biotechnology, Government of India.

The assays were performed in triplicate at each concentration to ensure reproducibility and statistical validity. A fluorescence-based detection method was employed to assess the cytotoxic potential of the test compounds. The method involved staining viable cells with fluorescent dyes, enabling quantification of cell viability post-treatment. This technique is known for its sensitivity and ability to provide reliable results across a wide range of cell types. Doxorubicin, a clinically established anticancer agent, was used as the positive control to benchmark the activity of the test compounds. The standard served as a reference for comparing the efficacy of the synthesized compounds under identical experimental conditions [11].

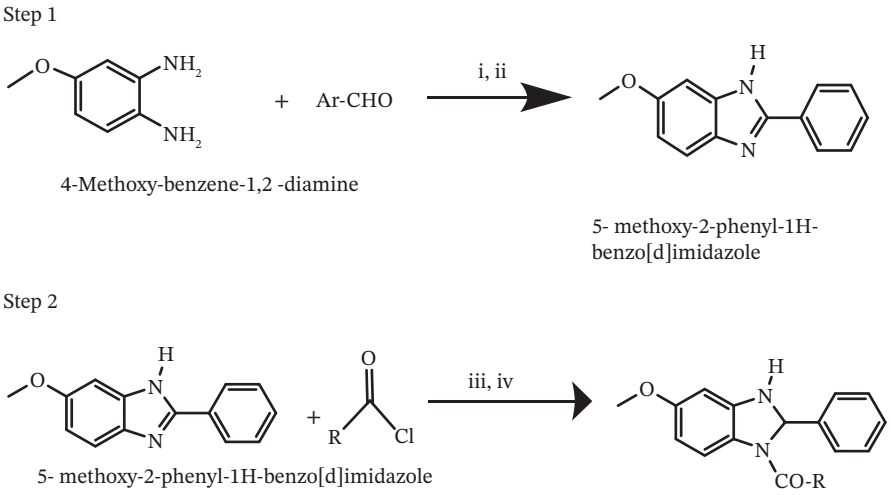

SCHEME 1 | Reaction condition: Step I (i) ammonium chloride (4 mmol); (ii) chloroform (5 mL) stir 5 min. Step II (iii) K_2CO_3 (2 mmol); (iv) DMF (10 ML) at 80°C for 4–6 h.

The anticancer potential of the compounds was quantified by calculating the percentage of cell growth inhibition at various concentrations. Furthermore, the half-maximal inhibitory concentration (IC_{50}) values were determined for each compound. IC_{50} represents the concentration of the compound required to inhibit 50% of cell growth, serving as a critical parameter to compare the potency of different molecules.

2.1.8.1 | MTT Reagent. MTT reagent (Catalog No. 11465007001) which contains 3-[4,5-dimethylthiazol-2-yl]-2,5-diphenyltetrazolium bromide) (1 x), at 5 mg/mL in phosphate-buffered saline (PBS, 806552) [12].

2.1.8.2 | RPMI 1640 (R0883) Culture Medium. PMI 1640 (R0883) containing 10% heat-inactivated FCS (fetal calf serum, 12106C), 2 mM glutamine (G6392), and 1 μg/mL actinomycin C1 (actinomycin D, A9415) [13].

The number of live cells after treating three DLM concentrations (1, 10, and 100 μM) was determined by MTT assay [14]. The relative survival rate was calculated as the percentage of control cells. The cells (1×10^4) were seeded in 96-well plates and incubated with DLM for 6 and 18 h at 37°C in a CO_2 incubator. Ten microliters of MTT (5 mg/mL PBS) was added, 4 h before completion of the incubation time, followed by centrifugation at 1200 x g for 10 mins. After removing the supernatant, 100 μL of dimethyl sulfoxide (DMSO) was added. The cell viability was measured utilizing the CellTiter 96 Proliferation Assay Kit (Promega, Madison, WI, USA) as indicated by the manufacturer's guidelines. The absorbance values were estimated using a Microplate Reader (Model 680, Bio-Rad) at 490 nm. The impact on cell viability at various concentrations of the compound was indicated as a %age by contrasting absorbances of treated cells and those of cells incubated with culture medium alone [15, 16]. The %cell growth inhibition and half-maximal inhibitory concentration (IC_{50}) values were resolved utilizing Prism programming (GraphPad Software, San Diego, CA) [17, 18].

3 | Results

3.1 | Spectral Analysis: Characterization of the Synthesized Molecules C1-C9 is Done as per the Spectra Displayed in the Supporting File. The FT-IR, ^{1}H-NMR, ^{13}C-NMR, and Mass Spectra of C1-C9 are in the Supporting File

3.1.1 | Characterization Data for (4-Fluoro-3-(Trifluoromethyl)Phenyl) (5-Methoxy-2-Phenyl-1H-Benzo[d]Imidazole-1-yl)Methanone (C1)

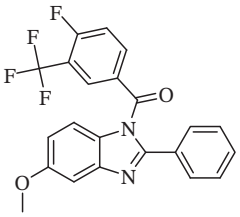

White solid (324 mg, yield 78%) **M.P.:** 185°C–187°C, **IR (DCM, cm^{-1}):** 3275, 3059, 1670, 1512, 1462, 1411, 1307, 1219, 837, 744, 501. ^{1}H NMR (400 MHz, $CDCl_3$, δ, ppm): 8.27 (s, 1H), 8.04–7.98 (t, 2H), 7.85 (d, J = 8.6 Hz, 2H), 7.53–7.46 (m, 2H), 7.27 (d, J = 10.1 Hz, 2H), 7.13 (d, 2H), 3.83 (s, 3H). **^{13}C NMR (100 MHz, $CDCl_3$, δ, ppm):** 169.6, 161.7, 161.7, 161.6, 161.6, 159.7, 159.7, 159., 159.5, 158.0, 154.1, 142.5, 133.8, 133.8, 132.1, 130.3, 128.6, 128.5, 115.9, 114.6, 100.6, 55.3 MS (ESI-TOF, m/z): $[M+H]^+$ Calcd: 415.10, Found: 415.12.

3.1.2 | (2-Fluorophenyl) (5-Methoxy-2-Phenyl-1H-Benzo[d]Imidazole-1-yl)Methanone (C2)

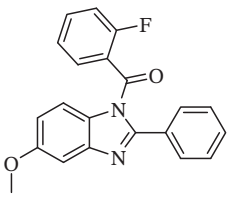

TABLE 2 | Substituted acyl derivatives.

Symbols	Structure
C1	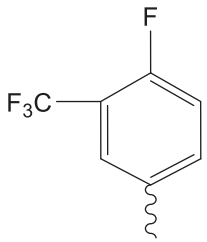
C2	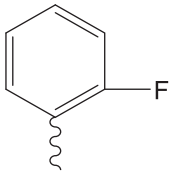
C3	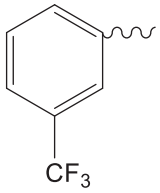
C4	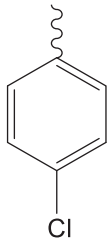
C5	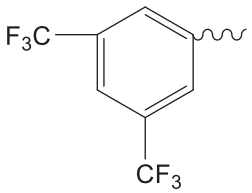
C6	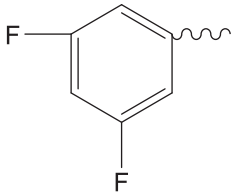
C7	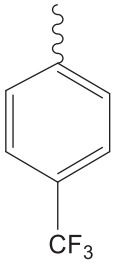

(Continues)

TABLE 2 | (Continued)

Symbols	Structure
C8	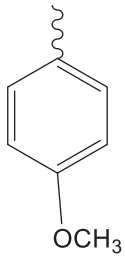
C9	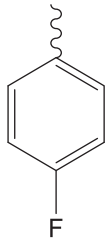

White solid (292 mg, yield 84%); m.p. = 173°C–175°C; IR (DCM, cm^{-1}): 3321, 3062, 1681, 1546, 1504, 1462, 1219, 833, 744, 516; ^1H NMR (400 MHz, $CDCl_3$): δ 8.27 (s, 1H), 8.04–7.98 (m, 2H), 7.85 (d, J = 8.6 Hz, 2H), 7.53–7.46 (m, 3H), 7.27 (d, J = 10.1 Hz, 2H), 7.13 (s, 2H), 3.83 (s, 3H); ^{13}C NMR (100 MHz, $CDCl_3$) δ 165.3, 165.2, 160.6, 158.6, 158.0, 154.6, 142.6, 132.5, 132.4, 132.2, 131.2, 130.3, 129.6, 128.5, 125.4, 121.6, 117.1, 115.9, 114.6, 100.5, 55.3; MS (ESI-TOF) m/z: $[M+H]^+$calcd347.11, found 347.21.

3.1.3 | [3-(Trifluoromethyl)Phenyl] (5-Methoxy-2-Phenyl-1H-Benzimidazol-1yl) Methanone (C3)

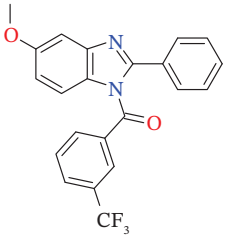

White solid (294 mg, yield 74%); **m.p.** = 179°C–181°C; **IR (DCM, cm^{-1}):** 3275, 3097, 1681, 1589, 1527, 1469, 1392, 1296, 1238, 1134, 1026, 867, 817, 748, 694, 443; ^1H NMR (400 MHz, $CDCl_3$): δ 8.27 (s, 1H), 8.04–7.98 (m, 2H), 7.85 (d, J = 8.6 Hz, 2H), 7.53–7.46 (m, 3H), 7.27 (d, J = 10.1 Hz, 2H), 7.13 (s, 2H), 3.83 (s, 3H); ^{13}C NMR (100 MHz, $CDCl_3$) δ 169.8, 158.0, 154.1, 142.5, 133.8, 133.8, 133.7, 133.7, 132.1, 131.8, 131.5, 131.2, 131.0, 130.3, 130.0, 129.0, 128.6, 128.5, 115.9, 114.6, 100.6, 55.3; MS (ESI-TOF) m/z: $[M+H]^+$calcd 397.11, found 397.09.

3.1.4 | (4-Chlorophenyl) (5-Methoxy-2-Phenyl-1H-Benzimidazol-1-yl)Methanone (C4)

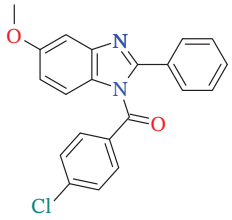

White solid (181 mg, yield 52%); m.p. = 159°C–161°C; IR (DCM, cm^{-1}):3255, 3186, 2962, 2873, 1697, 1612, 1516, 1462, 1415, 1311, 1253, 833, 744, 543; ^{1}H NMR (400 MHz, $CDCl_3$): δ 8.27 (s, 1H), 8.04–7.98 (m, 2H), 7.85 (d, J = 8.6 Hz, 2H), 7.53–7.46 (m, 3H), 7.27 (d, J = 10.1 Hz, 2H), 7.13 (s, 2H), 3.83 (s, 3H); ^{13}C NMR (100 MHz, $CDCl_3$) δ 169.1, 158.0, 154.1, 142.5, 137.1, 132.3, 132.1, 131.3, 130.3, 129.17, 129.0, 128.6, 128.5, 115.9, 114.6, 100.6, 55.3; MS (ESI-TOF) m/z: $[M+H]^+$calcd 363.81, found 364.07.

3.1.5 | 3,5-Bis[(Trifluoromethyl)Phenyl](5-Methoxy-2-Phenyl-1H-Benzimidazol-1-yl) Methanone (C5)

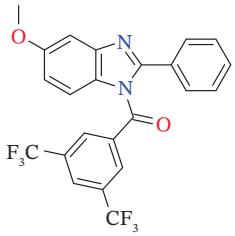

White solid (353 mg, 76%); m.p. = 193°C–195°C; IR (DCM, cm^{-1}):3275, 3097, 1681, 1589, 1527, 1469, 1392, 1296, 1238, 1134, 1026, 867, 817, 748, 694, 443; ^{1}H NMR (400 MHz, $CDCl_3$):δ 8.18 (d, J = 2.2 Hz, 2H), 8.04–7.96 (m, 3H), 7.85 (d, J = 8.6 Hz, 1H), 7.54–7.46 (m, 3H), 7.15–7.00 (m, 2H), 3.83 (s, 3H); ^{13}C NMR (100 MHz, $CDCl_3$) δ 169.1, 169.1, 169.0, 164.4, 164.3, 162.4, 162.3, 158.0, 154.2, 142.5, 134.8, 134.8, 132.1, 130.3, 129.3, 128.6, 128.5, 115.8, 114.7, 114.7, 108.5, 100.6, 55.3; MS (ESI-TOF) m/z: $[M+H]^+$calcd465.10, found 465.06.

3.1.6 | (3,5-Di-Fluorophenyl) (5-Methoxy-2-Phenyl-1H-Benzimidazol-1-yl) Methanone (C6)

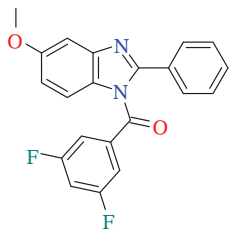

White solid (234 mg, 64%); m.p. = 168°C–170°C; IR (DCM, cm^{-1}): 3275, 3059, 1670, 1512, 1462, 1411, 1307, 1219, 837, 744, 501; ^{1}H NMR (400 MHz, $CDCl_3$): δ 8.18 (d, J = 2.2 Hz, 2H), 8.04–7.96 (m, 3H), 7.85 (d, J = 8.6 Hz, 1H), 7.54–7.46 (m, 3H), 7.15–7.00 (m, 2H), 3.83 (s, 3H); ^{13}C NMR (100 MHz, $CDCl_3$) δ 169.1169.1, 169.0, 164.4, 164.3, 162.4, 162.3, 158.0, 154.2, 142.5, 134.8, 134.8, 134.7, 132.1, 130.3, 128.6114.7, 115.8, 108.1, 100.6, 55.3; MS (ESI-TOF) m/z: $[M+H]^+$calcd 365.11, found 365.12.

3.1.7 | (5-Methoxy-2-Phenyl-1H-Benzimidazol-1-yl) [4-(Trifluoromethyl) Phenyl] Methanone (C7)

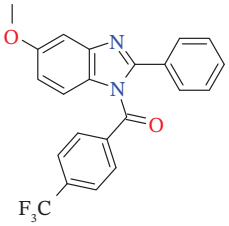

White solid (207 mg, 52%); m.p. = 168°C–170°C; IR (DCM, cm^{-1}):3271, 3059, 1666, 1554, 1512, 1408, 1226, 837, 740, 513; ^{1}H NMR (400 MHz, $CDCl_3$): δ 8.00 (d, J = 5.5 Hz, 2H), 7.91 (s, 4H), 7.84 (d, J = 8.8 Hz, 1H), 7.52–7.47 (m, 3H), 7.15–7.02 (m, 2H), 3.83 (s, 3H); ^{13}C NMR (100 MHz, $CDCl_3$) δ 169.4, 158.0, 154.1, 142.5, 134.3, 132.9132.6, 132.4, 132.1, 132.1, 130.3, 130.3, 130.2, 130.2, 130.22, 129.08, 128.6, 127.1, 126.3, 115.9, 100.6, 55.3; MS (ESI-TOF) m/z: $[M+H]^+$calcd 397.11, found 397.17.

3.1.8 | (4-Methoxy Phenyl) (5-Methoxy-2-Phenyl-1H-Benzimidazol-1-yl) Methanone (C8)

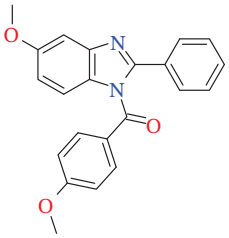

White solid (273 mg, 76%); m.p. = 172°C–174°C; IR (DCM, cm^{-1}):3255, 3186, 2962, 2873, 1697, 1612, 1516, 1462, 1415, 1311, 1253, 833, 744, 543; ^{1}H NMR (400 MHz, $CDCl_3$): δ 8.03–7.97 (m, 2H), 7.93–7.82 (m, 3H), 7.53–7.46 (m, 3H), 7.16–7.00 (m, 4H), 3.83 (s, 3H), 3.80 (s, 3H); ^{13}C NMR (100 MHz, $CDCl_3$) δ 169.6, 162.5, 158.0, 154.1, 142.5, 132.1, 131.3, 130.3, 129.0, 128.6, 128.5, 128.2, 115.91, 114.69, 113.5, 100.6, 55.3, 55.3; MS (ESI-TOF) m/z: $[M+H]^+$calcd 359.14, found 359.12.

3.1.9 | (4-Fluorophenyl) (5-Methoxy-2-Phenyl-1H-Benzimidazol-1-yl) Methanone (C9)

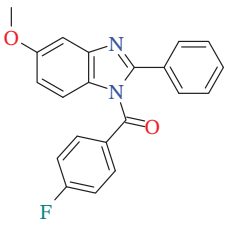

White solid (305 mg, 88%); m.p. = 173°C–175°C; IR (DCM, cm^{-1}): 3271, 3059, 1666, 1554, 1512, 1408, 1226, 837, 740, 513; ^{1}H NMR (400 MHz, $CDCl_3$): δ 8.03–7.98 (m, 2H), 7.90–7.82 (m, 3H), 7.50 (s, 3H), 7.35–7.27 (m, 2H), 7.15–7.01 (m, 2H), 3.83 (s, 3H); ^{13}C NMR (100 MHz, $CDCl_3$) δ 169.5, 166.1, 164.1, 158.0, 154.1, 142.5, 132.2, 132.2, 132.1, 130.4, 130.4, 130.3, 129.0, 128.6, 128.5,

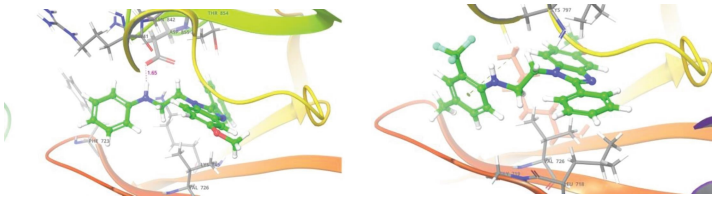

(a) (b)

FIGURE 1 | Molecular docking studies reveal the binding orientations of molecules. (a) Compound C7 and (b) Compound C1 within the active site of the EGFR kinase enzyme (PDB ID: 3 W2S). The ligand molecules are depicted in a bold stick representation, with carbon atoms in green, while interacting residues within a 4.0-Å radius are shown using stick and wire representations, with carbon atoms in gray. Hydrogen bonding interactions are indicated by magenta dotted lines, along with the corresponding distances in angstroms (Å).

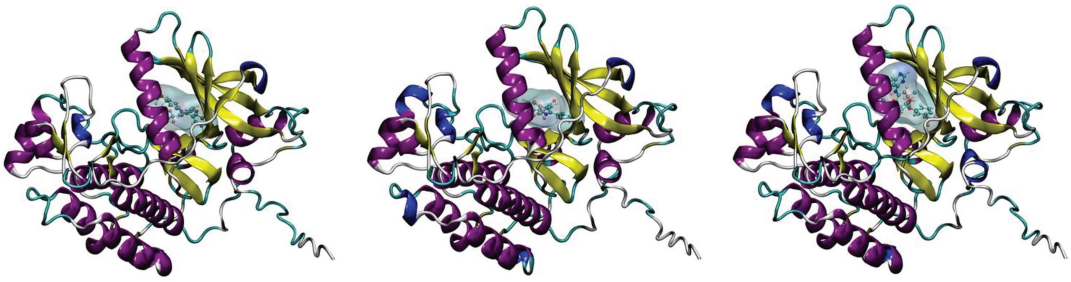

(a) (b) (c)

FIGURE 2 | Molecular docking studies reveal the binding orientations of molecules. (a) Compound C1, (b) Compound C7, and (c) TAK-285-EGFR complex within the active ATP-binding site of the EGFR (PDB ID: 3RCD).

115.9, 115.6, 115.4, 114.6, 100.6, 55.3; MS (ESI-TOF) m/z: $[M+H]^+$calcd 347.12, found 347.1.

The derivatives synthesized had NH peak in 3300-3400 cm^{-1}, CH peaks in 2800–3100 cm^{-1}, and CN peaks in 1650- 1590 cm^{-1} in FT-IR spectroscopy, whereas in all the ^1H NMR, the NH peak was in the range of 5–6 ppm and 7–8 ppm for aromatic hydrogens and 3–4 ppm for aliphatic methyl groups.

3.2 | Molecular Docking

The evaluation of molecule binding within the active site of the EGFR kinase was done by SP docking. C7 and C1 have exhibited strong interactions with the catalytic residues. These interactions primarily involved hydrogen bonding and hydrophobic interactions (PDB ID: 3 W2S and PDB:3RCD) (Figures 1, 2, 3). Tables 3 and 4 display the top hit docking score.

3.3 | Evaluation of Synthesized Molecules for *In Vitro* Anticancer Activity

The synthesized compounds **(C1–C9)** were subjected to *in vitro* anticancer activity assays using whole-cell models of MCF-7 (human breast adenocarcinoma), HeLa (cervical cancer), and A549 (non–small cell lung carcinoma, NSCLC) cell lines. The assays were designed to assess the percentage of viable cells after treatment with the test compounds, and the results were compared against untreated controls to determine cytotoxic efficacy. Doxorubicin, a widely used standard anticancer agent, served as the positive control for benchmarking the activity of the synthesized compounds.

The evaluation was conducted across a broad concentration range (0.625 to 300 μg/mL), providing a comprehensive understanding of the dose–response relationship for each compound. The activity was quantified by measuring cell viability at each concentration, and the results were expressed as a percentage of cell growth inhibition relative to the control. Graphical representations of the % growth inhibition against the concentration of each compound were plotted for MCF-7, HeLa, and A549 cell lines (Figures 4, 5, 6).

The results demonstrated that five compounds, namely C1, C2, C3, C5, and C7, exhibited notable anticancer activity across all tested cell lines. This observation was further validated by estimating the half-maximal inhibitory concentration (IC_{50}) values for each compound. Notably, compounds C1, C2, C3, C5, and C7 displayed IC_{50} values below 50 μM, indicating their significant cytotoxic potential (Table 5). These IC_{50} values were comparable to those of doxorubicin, emphasizing the efficacy of these compounds as potential anticancer agents.

4 | Discussion

The anticancer activity observed suggests a promising structure–activity relationship (SAR) for the active compounds. Specifically, variations in molecular structure appear to influence the interaction of these compounds with cellular targets, resulting in differential efficacy against the cancer cell lines. The chemical structures of the compounds exhibiting the highest anticancer potency against MCF-7 (breast cancer), HeLa (cervical cancer), and A549 (non–small cell lung carcinoma) cell lines are presented in Figure 7. Among the nine

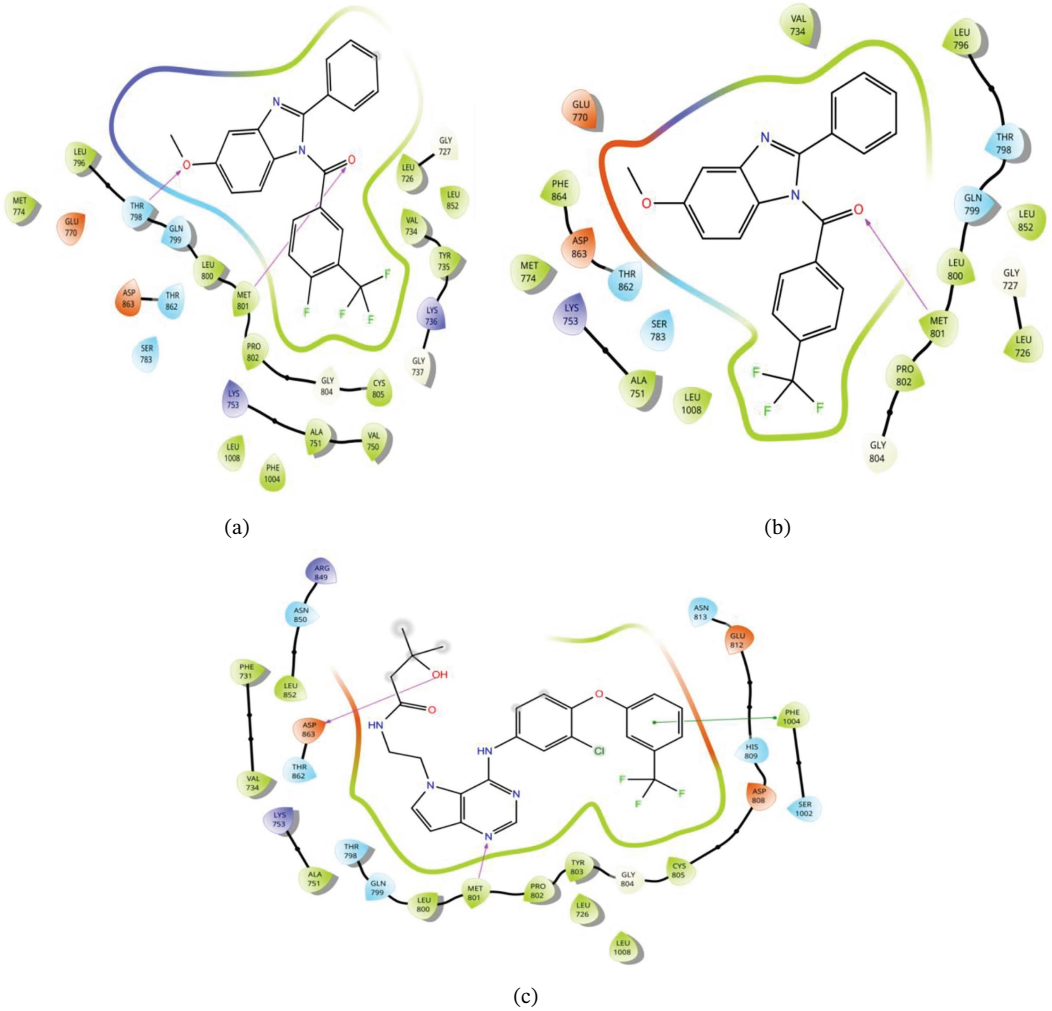

FIGURE 3 | 2D molecular docking poses of molecules. (a) Compound C1, (b) Compound C7, and (c) TAK-285-EGFR complex within the active ATP-binding site of the EGFR (PDB ID: 3RCD).

TABLE 3 | Molecular docking studies of top hit molecules inside the active site of EGFR kinase (PDB ID: 3 W2S).

Sr.	Molecule	Docking score (kcal/mol)	eModel score	Interactions
1.	C7	−6.040	−51.114	H-bond interaction with ASP800 and hydrophobic interactions with LEU718, ALA722, CYS797, and LEU844
2.	C1	−4.520	−44.117	H-bond interaction with ASP800 and hydrophobic interactions with LEU718, VAL726, CYS797, and PHE997

TABLE 4 | Molecular docking studies of top hit molecules inside the active site of EGFR kinase (PDB ID: 3CRD).

Sr.	Ligand	Docking score (kcal/mol)	eModel score	H-bond interactions
1.	C1	−9.280	−78.36	H-bond interaction withTHR798 and MET801
2.	C7	−9.250	−78.00	H-bond interaction with MET801
3.	TAK-285	−8.338	−69.70	H- bond interaction with MET801 and ASP863 Pi-stacking interactions with PHE1004

synthesized derivatives (C1–C9), five compounds—C1, C2, C3, C5, and C7—demonstrated significant anticancer activity, as indicated by their IC_{50} values falling below the 50 μM threshold. This level of activity suggests that these compounds possess a promising cytotoxic profile against the tested cancer cell lines.

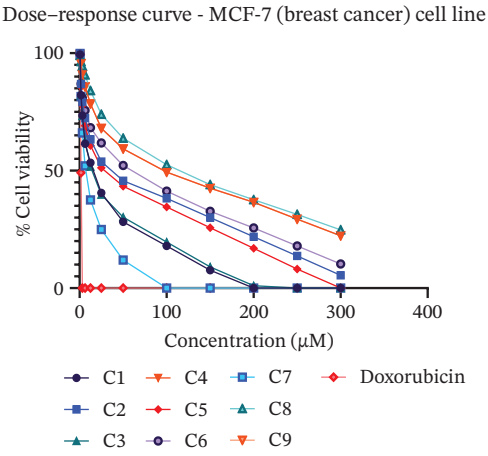

FIGURE 4 | Effect of Compounds **C1–C9** and doxorubicin against the MCF-7 cell line viability. The plot represents the data in terms of % growth vs. concentration.

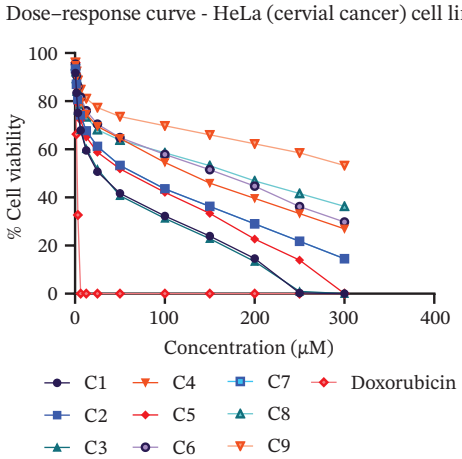

FIGURE 5 | Effect of Compounds **C1–C9** and doxorubicin against the HeLa cell line viability. The plot represents the data in terms of % growth vs. concentration.

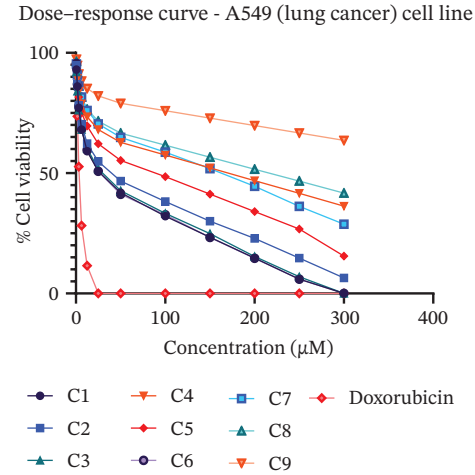

FIGURE 6 | Effect of Compounds **C1–C9** and doxorubicin against the A549 cell line viability. The plot represents the data in terms of % growth vs. concentration.

TABLE 5 | IC_{50} of Compounds **C1–C9** and doxorubicin against MCF-7, HeLa, and A549 cell lines.

Sr.	Molecule	IC_{50}[a] (μM) MCF-7[b] (μM)	IC_{50}[a] (μM) HeLa[c] (μM)	IC_{50}[a] (μM) A549[d] (μM)
1.	C1	20.6 ± 1.6	25.3 ± 2.1	16.6 ± 2.3
2.	C2	45.1 ± 4.2	30.7 ± 2.8	45.4 ± 5.1
3.	C3	18.4 ± 1.2	22.1 ± 1.5	24.5 ± 1.7
4.	C4	225.7 ± 8.5	85.9 ± 5.3	98.2 ± 6.9
5.	C5	22.8 ± 1.9	18.6 ± 2.2	31.9 ± 2.5
6.	C6	58.4 ± 4.8	65.5 ± 5.4	52.1 ± 4.9
7.	C7	9.2 ± 0.5	56.7 ± 5.8	63.3 ± 3.9
8.	C8	256.8 ± 15.7	130.4 ± 7.2	75.7 ± 4.1
9.	C9	223.5 ± 12.4	265.3 ± 16.5	165.9 ± 7.4
10.	Doxorubicin (standard)	1.2 ± 0.3	0.8 ± 0.2	1.7 ± 0.4

[a]50% inhibitory concentration.
[b]MCF-7 (breast cancer).
[c]HeLa (cervical cancer).
[d]A549 (non–small-cell lung carcinoma).

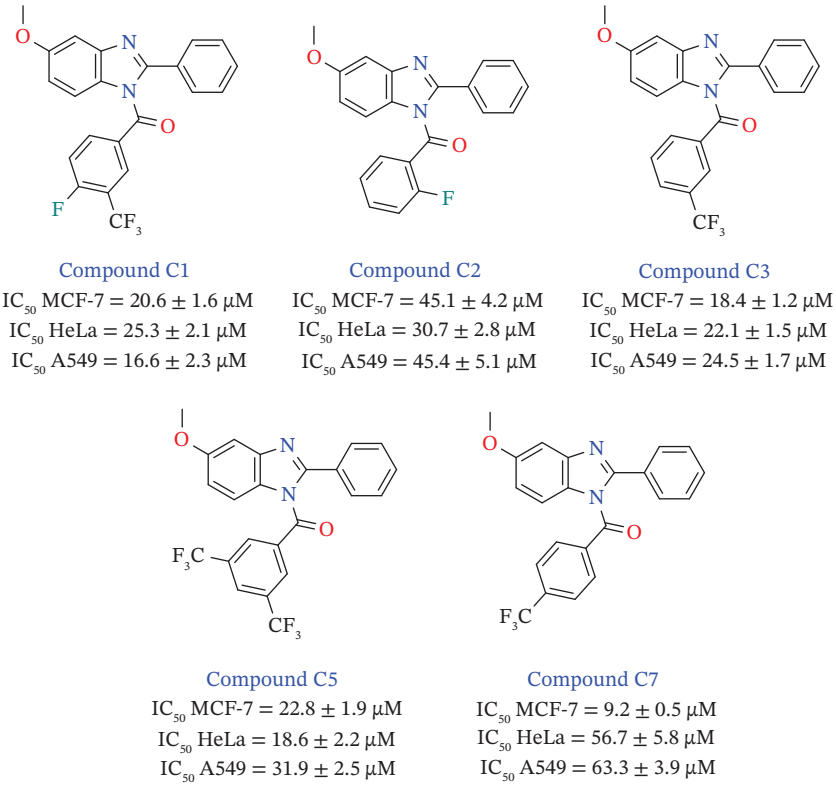

FIGURE 7 | The structure of compounds which displayed the highest potency against MCF-7 (breast cancer), HeLa (cervical cancer), and A549 (lung cancer) cell lines.

Among the active derivatives, compounds **C7** and **C1** emerged as the most potent candidates. Compound C7 exhibited exceptional activity, with an IC_{50} value of $\mathbf{9.2 \pm 0.5\ \mu M}$ against the MCF-7 cell line, highlighting its potential as a strong candidate for breast cancer therapy. Similarly, compound C1 demonstrated notable potency against the A549 cell line, with an IC_{50} value of $\mathbf{16.6 \pm 2.3\ \mu M}$, underscoring its efficacy against lung cancer. These values signify the promising selective activity of these derivatives across different cancer types.

In comparison, the standard anticancer agent **doxorubicin** exhibited superior potency, with IC_{50} values ranging from **0.8 to 1.7 μM** across all tested cell lines. While doxorubicin's efficacy is unparalleled, the observed activity of the synthesized compounds, particularly C7 and C1, reflects their potential as promising lead molecules for anticancer drug development. The structural analysis of these compounds indicates that specific molecular features may contribute to their enhanced anticancer activity. These findings highlight the need for further optimization and mechanistic studies to improve their potency and selectivity.

5 | Conclusion

In conclusion, the *in silico* results displayed that C1 and C7 were the top hits and had better binding affinity with the ATP-binding site of the EGFR kinase in breast cancer. The synthesized compounds **C1–C9** were systematically evaluated for their *in vitro* anticancer activity against MCF-7 (breast cancer), HeLa (cervical cancer), and A549 (lung cancer) cell lines. Five compounds—C1, C2, C3, C5, and C7—demonstrated significant anticancer potential with IC_{50} values below 60 μM, indicating notable cytotoxic efficacy. Among these, compounds C7 and C1 stood out as the most potent, with IC_{50} values of 9.2 ± 0.5 μM and 16.6 ± 2.3 μM against the MCF-7 and A549 cell lines, respectively, while the standard drug doxorubicin exhibited superior potency, with IC_{50} values in the range of 0.8–1.7 μM. However, the activity profiles of C7 and C1 underscore their promise as potential lead compounds for further development. These findings pave the way for in-depth mechanistic studies, structural optimization, and preclinical evaluations to fully explore their potential as novel anticancer agents.

Funding

No funding was received for this manuscript.

Conflicts of Interest

The authors declare no conflicts of interest.

Data Availability Statement

The data that support the findings of this study are available in the supporting information of this article.

References

1. K. Kyriakopoulou, E. Kefali, Z. Piperigkou, H. Bassiony, and N. K. Karamanos, "Advances in Targeting Epidermal Growth Factor Receptor Signaling Pathway in Mammary Cancer," *Cellular Signalling* 51 (2018): 99–109, https://doi.org/10.1016/j.cellsig.2018.07.010.

2. S. L. Klein and K. L. Flanagan, "Sex Differences in Immune Responses," *Nature Reviews Immunology* 16, no. 10 (2016): 626–638, https://doi.org/10.1038/nri.2016.90.

3. *World Health Organization* (21 July 2021), https://who.int/data/gho/data/theme/mortality-and-global%2013health%2013estimate/.

4. H. Sung, J. Ferlay, R. L. Siegel, et al., "Global Cancer Statistics 2020: GLOBOCAN Estimates/of Incidence and Mortality Worldwide for 36 Cancers in 185 Countries," *CA: A Cancer Journal for Clinicians* 71, no. 3 (2021): 209–249, https://doi.org/10.3322/caac.21660.

5. J. B. Wright, "The Chemistry of Benzimidazole," *Chemistry Review* 48, no. 3 (1951): 397–541, https://doi.org/10.1021/cr60151a002.

6. R. S. Keri, A. Hiremathad, S. Budagumpi, and B. M. Nagaraja, "Comprehensive Review in Current Developments of Benzimidazoles-Based Medicinal Chemistry," *Chemical Biology & Drug Design* 86, no. 1 (2015): 19–65, https://doi.org/10.1111/cbdd.12462.

7. E. Vitaku, D. T. Smith, and J. T. Njardarson, "Analysis of the Streuctural Diversity, Substitution Pattern and Frequency of Nitrogen Heterocycles Among U.S.FDA Approved Pharmaceuticals," *Journal of Medicinal Chemistry* 57, no. 24 (2014): 10257–10274, https://doi.org/10.1021/jm501100b.

8. V. Ss Gupta, D. T. Nanna panei, and M. I. Reddy, "Synthesis, Characterization and Biological Evaluation of Benzimidazole Derivative as Potential Anixiolytic," *Journal of Young Pharmacist* 2, no. 3 (July-september 2010): 273–279.

9. S. L. Zhang, G. L. Damu, L. Zhang, R. X. Geng, and C. H. Zhou, "Synthesis and Bilogical Evaluation of Novel Benzimidazole Derivatives and Their Binding Behavoir With Bovine Serum Albumin," *European journal of medicinal Chemistry* 55 (September 1 2012): 164–175.

10. A. Bistrvic, L. Krstulovic, A. Harej, et al., "Design Ssynthesis and Biological Evaluation of Novel Benzimidazole Amidines as Potent Multi-Target Inhibitors for the Treatmet of Non-Small Cell Lung Cancer," *European Journal of Medicinal Chemistry* 143 (January 1 2018): 1616–1634.

11. J. Lao, J. Madani, T. Puértolas, et al., "Liposomal Doxorubicin in the Treatment of Breast Cancer Patients: A Review," *Journal of Drug Delivery and Therapeutics* 2013, no. 1 (2013): 456409–456412, https://doi.org/10.1155/2013/456409.

12. R. Supino, *MTT Assays BT–In Vitro Toxicity Testing Protocols*, ed. S. O'Hare and C. K. Atterwill (Totowa, NJ: Humana Press, 1995), 137–149, https://doi.org/10.1385/0-89603-282-5:137.

13. K. Awasthi, F.-L. Chang, P.-Y. Hsieh, H.-Y. Hsu, and N. Ohta, "Characterization of Endogenous Fluorescence in Nonsmall Lung Cancerous Cells: A Comparison With Nonmalignant Lung Normal Cells," *Journal of Biophotonic* 13, no. 5 (2020): e201960210, https://doi.org/10.1002/jbio.201960210.

14. T. Mosmann, "Rapid Colorimetric Assay for Cellular Growth and Survival: Application to Proliferation and Cytotoxicity Assays," *Journal of Immunological Methods* 65, no. 1-2 (1983): 55–63, https://doi.org/10.1016/0022-1759(83)90303-4.

15. V. Sharma, A. Kumar, R. Rawat, et al., "Computational Insights Into KRAS G12C Inhibition: Exploring Possible Repurposing of Azacitidine and Ribavirin," *Journal of Biomolecular Structure Dynamics* 43, no. 16 (2025): 1–11, https://doi.org/10.1080/07391102.2024.2321237.

16. F. Siddique, A. Aqdas, M. Bashir, et al., "Harnessing the Potential of Natural Products in Cancer Treatment: A Comprehensive Review," *Journal of Biological Regulators & Homeostatic Agents*, 38, no. 2, 873–897.

17. M. Sanduja, J. Gupta, R. Rawat, U. Singh, and S. M. Verma, "Designing, Molecular Docking, and Dynamics Simulations Studies of 1,2,3-Triazole Clamped Uracil–Coumarin Hybrids against EGFR Tyrosine Kinase," *Journal of Applied Pharmaceutical Science* 10, no. 3 (2020): 001–011.

18. S. A. Arvindekar, S. Mohole, A. Patil, et al., "Molecular Docking, QSAR, Pharmacophore Modeling, and Dynamics Studies of Some Chromone Derivatives for the Discovery of Anti-Breast Cancer Agents Against Hormone-Dependent Breast Cancer," *Journal of Biomolecular Structure Dynamics* 41, no. 24 (2023): 14757–14770, https://doi.org/10.1080/07391102.2023.2190803.

Supporting Information

Additional supporting information can be found online in the Supporting Information section. **Supporting Information.** Supporting information has been attached which displays spectra of the novel synthesized small molecules. Characterization of these molecules C1–C9 is done as per the spectra in the supporting file. The FT-IR spectra 1H- NMR; 13C -NMR and mass spectra of C1–C9.